Lantern-Explorer: A Collision-Avoidance Autonomous Exploration Drone System Based on Laser SLAM with Optimized Hardware and Software

Lei Zhu[1,2], Ruofei Zhong[1,2], Donghai Xie[1,2], Xinze Yuan[1,2]

[1] College of Resource Environment and Tourism, Capital Normal University, Beijing, China - y2n80d@gmail.com, zrfsss@163.com, (6121, 2230902171)@cnu.edu.com
[2] Key Laboratory of 3D Information Acquisition and Application, Ministry of Education, Capital Normal University, Beijing, China

Keywords: LiDAR SLAM, autonomous exploration, FUEL-360, Adaptive linear controller, 3D mapping in complex environments.

Abstract

The inherent high flexibility of drone platforms has positioned them as a powerful tool when combined with LiDAR technology for acquiring three-dimensional data in confined spaces. However, due to limitations in onboard resources, energy, and flight stability, improving autonomous exploration efficiency and mapping accuracy has remained a challenge. To address this, we propose Lantern-Explorer, an autonomous exploration drone system optimized for both hardware and software based on LiDAR SLAM, to balance exploration efficiency and mapping accuracy in complex environments. The hardware design includes a compact, highly maneuverable, and stable coaxial dual-rotor octocopter platform with passive collision avoidance capabilities. A custom-developed flight controller supports high-bandwidth IMU data feedback to enhance the precision of the tightly-coupled LiDAR-inertial mapping module. On the software side, we designed an adaptive LiDAR odometry accuracy controller to achieve precise flight attitude control, ensuring high-speed flight while maintaining stability. Additionally, we proposed the improved omnidirectional LiDAR perception algorithm, FUEL-360, for autonomous exploration. This algorithm, based on the LiDAR FOV model, optimizes the strategy for detecting unknown frontiers, improving the efficiency of boundary extraction and viewpoint generation. By employing a viewpoint classification strategy based on a dual-nested Traveling Salesman Problem, it reduces redundant backtracking during exploration, ensuring the rationality of local and global path planning and thereby enhancing overall exploration efficiency. To verify the effectiveness of the optimized hardware and software design, extensive experiments were conducted in complex environments such as forests, tunnels, and underground parking lots. Compared with existing platforms and methods, Lantern-Explorer demonstrated significant advantages in both exploration efficiency and mapping accuracy. Experimental results indicate that the system has substantial engineering potential in real-world applications, providing a comprehensive and innovative solution for autonomous drone exploration in complex environments. The relevant software and hardware resources will be open-sourced at https://github.com/R7AY/Dream-Lantern to promote further research in the field.

1. Introduction

Compared with traditional Mobile Mapping Systems (MMS) and Personal Laser Scanning Systems (PLS), Unmanned Aerial Vehicle (UAV), Laser Scanning Systems (ULS) leverage superior maneuverability to access narrow or hazardous areas that are difficult for humans to reach. This capability has led to their widespread use in disaster search (Peng et al., 2024) and rescue(Kim et al., 2024), resource exploration(Wang B et al., 2024), industrial inspection(Wang C et al., 2024), and environmental monitoring(Zhang et al., 2024). However, conventional drones often utilize vehicle-mounted LiDAR sensors, which, due to their size and weight, result in insufficient thrust-to-weight ratios. Additionally, their open design lacks compactness and collision protection(Kong et al.,), making stable and efficient autonomous exploration and mapping in complex, confined environments challenging.

In recent years, the emergence of MEMS semi-solid-state LiDARs such as the Livox Mid360 and Unitree L1 PM has greatly expanded research on UAV LiDAR perception(Chen et al., 2019). The high precision and miniaturization of these sensors facilitate more compact UAV designs, driving the development of ULS towards miniaturization and intelligence. However, the current market still lacks an open-source UAV platform that combines collision protection, lightweight design, flight stability, and redundant power to support related research and practical applications.

ULS has gained significant attention and research interest for its capability to replace humans in high-risk environments and build high-precision 3D maps. Autonomous mapping in unknown environments remains a research focus, as enhancing autonomous exploration ability is recognized as a highly complex and challenging task. Unlike photogrammetry tasks completed through pre-planned waypoints, autonomous exploration algorithms must autonomously extract the most information-rich viewpoints in real-time during mapping, determine the sequence for visiting these viewpoints, and achieve efficient environment sampling(Gul et al., 2023). While ULS benefits from three-dimensional motion and rotational degrees of freedom, the high flexibility can lead to overly aggressive movements that affect mapping accuracy. Balancing sampling efficiency and accuracy is a key challenge in practical applications.

For autonomous ULS, the structure of the UAV platform and sensor layout directly influence motion stability and data acquisition accuracy, particularly in complex environments. High-maneuverability flights may amplify IMU sensor errors, propagating to LiDAR point cloud data, causing odometry drift and impacting map accuracy. On the software side, the execution strategy of exploration algorithms directly affects overall exploration efficiency. Delays in path planning can lead to discrepancies between planned and actual movements, affecting exploration efficiency and mapping accuracy. While reducing UAV flight speed can enhance mapping accuracy to some extent, it sacrifices maneuverability and lowers overall exploration efficiency.

Balancing hardware design and algorithm optimization to ensure both mapping accuracy and exploration efficiency is a key focus of current research. Therefore, we propose the Lantern-Explorer, an autonomous UAV system optimized for both hardware and software, as shown in figure 1. The main contributions of Lantern-Explorer are as follows:

(1) A collision-resistant coaxial dual-rotor octocopter platform: The UAV body is made of lightweight carbon fiber and features anti-roll and collision protection functions. The propulsion system employs a coaxial dual-rotor octocopter design, making the body more compact, with high thrust redundancy and excellent flight stability. A high-performance flight controller, NxtPX4 V2s, was developed based on NxtPX4, capable of outputting IMU data streams at up to 500 Hz to enhance state estimation and mapping accuracy.
(2) Adaptive odometry precision linear controller: This component imposes real-time dynamic constraints on control inputs of linear and angular velocities for flight state management. A second-order low-pass filter further smooths control velocities, enabling real-time dynamic adjustments of speed and attitude during autonomous exploration to balance flight speed and exploration efficiency.
(3) Omnidirectional perception autonomous exploration and mapping algorithm: Leveraging the omnidirectional perception capability of LiDAR, we proposed FUEL-360, an improved version of the FUEL algorithm. This algorithm integrates the LiDAR field-of-view model, optimizing the extraction of frontier points to avoid redundant observations in global path planning and eliminating Z-axis drift due to frequent heading changes. The use of boundary classification techniques further prevents repeated exploration and backtracking, thereby enhancing overall exploration efficiency.
(4) Extensive experimental validation: To comprehensively evaluate the system's performance, we first designed mapping accuracy comparison experiments under fixed flight routes with different platforms to verify the rationale of the proposed hardware design. Subsequently, experiments were conducted in representative environments such as dense forests, tunnels, underground parking lots, and long corridors to assess the improvements brought by the exploration algorithm and adaptive odometry precision controller. The results demonstrated that Lantern-Explorer exhibited high autonomous exploration efficiency and point cloud mapping accuracy.

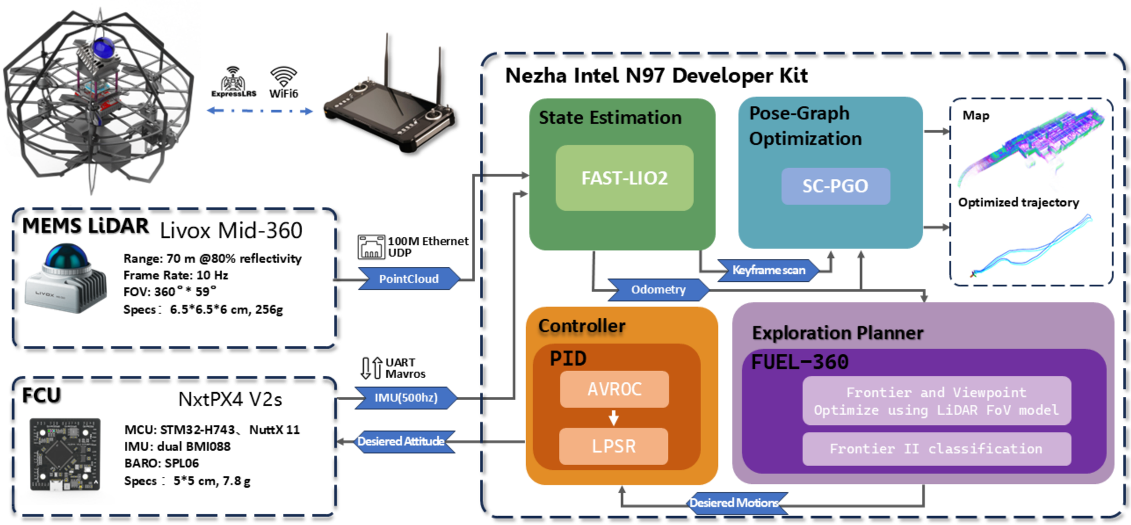

Figure 1. Overall System Architecture of Lantern-Explorer
Note: FAST-LIO2 is an open-source LiDAR-Inertial Odometry tightly coupled system developed by HKUST. In the controller, AVROC refers to the Adaptive Velocity Regulation for Odometry Covariance, a constraint module proposed in this paper for adaptive odometry accuracy. LPSR stands for Low-Pass Filter (LPF) and the smoothing processing module for second-order system responses.

2. Related Work

2.1 Design of UAV platform

Currently, many scholars have designed unique drone platforms based on their research needs (as shown in figure 2). The ASL-Flight is an early visual sensor-based quadcopter platform that uses multi-sensor fusion and Model Predictive Control (MPC) to achieve precise trajectory tracking and stable hovering, reducing development costs and enhancing research reproducibility. Agiliciou(Foehn et al., 2022) is designed for vision-guided agile quadcopter missions, offering a flexible hardware and software framework that supports multiple controllers and sensors. The Fast-Drone-250 is used for learning autonomous navigation algorithms like Ego-planner(Zhou et al., 2020), but its limited power redundancy and poor scalability restrict its application in complex engineering tasks. The UniQuad series(Zhang et al., 2024) integrates depth cameras and LiDAR, specifically designed for autonomous flight missions, demonstrating excellent trajectory tracking accuracy. The TerraLuma UAV-LiDAR(Wallace et al., 2012) is used for forestry and environmental monitoring, capable of generating high-precision 3D point clouds, but its large wheelbase limits flexibility. The MRS UAV system(Baca et al., 2021) supports multi-frame positioning and multi-sensor fusion, suitable for complex tasks in GNSS-denied environments, but its system complexity and integration limits widespread use.

Overall, vision-based drone platforms are compact but lack scalability, while LiDAR-based drone platforms have strong perception capabilities, making them ideal for large-scale environmental monitoring, though their complexity and cost limit their use in specific domains.

2.2 Autonomous exploration

Autonomous exploration is considered complex and challenging in the field of robotics. Past research has mainly focused on boundary-based (frontier) methods and sampling-based methods. The classic frontier exploration method, proposed by Yamauchi(Yamauchi et al., 1997), guides the robot's exploration by detecting the boundary between known and unknown spaces.

While suitable for simple environments, it may result in redundant backtracking in complex environments. Building on this, Zhou(Zhou et al., 2020) introduced the Incremental Frontier Information Structure (FIS), combining global path planning with local optimization to improve exploration efficiency. Gomez(Gomez et al., 2019) enhanced exploration efficiency and path optimization by integrating geometric, topological, and semantic information, using semantic frontier classification and cost-utility functions.

Sampling-based methods generate exploration paths via random sampling and select the optimal path based on information gain or cost-benefit criteria. Umari utilized multi-RRT (Rapidly-exploring Random Tree) for autonomous exploration, where local trees accelerate exploration of nearby areas, while global trees ensure coverage of distant regions, though this increases computational complexity. Zhu proposed a two-stage viewpoint planning(Zhu et al., 2021) approach, where a local RRT expands the known area, and a re-localization stage selects uncovered regions for further exploration. This method effectively covers complex environments, but in open or intricate settings, the re-localization mode may trigger inefficiently, requiring significant computational resources to maintain a global map.

3. Methodology

3.1 Hardware optimisation

3.1.1 Onboard computing Hardware Design

The Lantern-Explorer system aims to balance mapping accuracy and efficiency. It consists of three key hardware modules (as shown in figure 1). First, to ensure sufficient computational power, the system uses the Nezha X86 development board, equipped with a 3.6 GHz quad-core Intel N97 CPU, 8GB LPDDR5 RAM, and 64GB eMMC storage. Second, the onboard LiDAR is a 256g Livox Mid-360, which offers a 360° horizontal and 59° vertical field of view (FOV), improving localization accuracy and reducing heading angle variations, thereby enhancing SLAM mapping precision.

The improved NxtPX4 V2s flight controller uses two BMI088 MEMS IMUs, which outperform the built-in ICM40609 MEMS IMU in the Mid-360 LiDAR in terms of noise density, measurement bandwidth, dynamic range, and shock resistance. Consequently, we modified the PX4 firmware to implement a 500Hz Mavros topic return. The high-frequency IMU data supplement the laser-inertial odometry, aiding in point cloud motion compensation and frame-to-frame registration. The flight control parameters are marked in the lower-left dashed box in figure 1.

3.1.2 Power system and avionics layout.

Coaxial dual-rotor octocopters are widely used in industrial drones, offering higher payload capacity, precision, and stability compared to traditional quadcopters. With the same wheelbase, they provide greater motor redundancy and stronger thrust output, enabling high maneuverability in confined spaces. However, the lower rotors experience interference from the upper airflow, leading to a thrust loss of about 10%-20% (Bondyra et al., 2016). Given the redundancy and safety requirements for autonomous exploration tasks, this efficiency loss is acceptable. To minimize the impact, According to Bohorquez, the Lantern-Explorer's rotor plane must satisfy (Bohorquez et al., 2007):

$$\frac{h}{r_p} > 0.357 \tag{1}$$

where h is the distance between the upper and lower rotor planes, and r_p is the rotor blade radius.

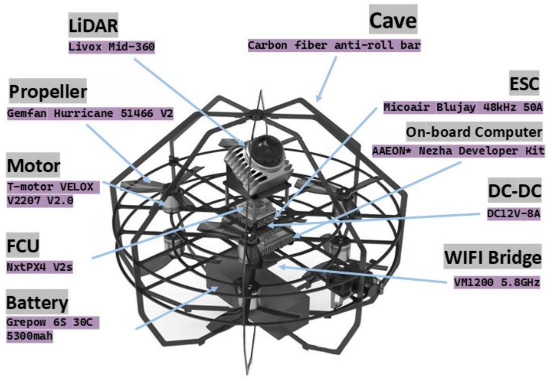

Figure 2. Lantern-Explorer Onboard Layout Diagram

The layout of onboard equipment affects the overall center of gravity (CG) of the drone. If the CG is below the rotor plane, the induced airflow generated by the wind will cause the pitch angle to diverge until the drone flips. Conversely, if the CG is above the rotor plane, the resistance opposite to the flight direction will also cause the pitch angle to diverge. According to practical considerations (Pierre et al., 2009), the CG of the Lantern-Explorer is positioned slightly below the lower rotor plane. To ensure that the LiDAR always receives ground reflections at a certain altitude and to prevent the loss of feature points leading to localization divergence, the LiDAR is rotated 25° downward around the Y-axis toward the nose of the drone. The final onboard hardware layout is shown in figure 2 , The final hardware layout and three-dimensional dimensions are shown in the figure 3 , with the measured performance parameters listed in the table 1.

Specific Parameters	Value
3D size（mm）	L:360×W:360×H:325
Weight (g)	1129(Battery not included)
Hover time (min)	12.3
TWR	6.21
Maximum efficiency throttle	40%
Power battery capacity	6S1P 22.2V 30C 5300mAh
telemetry distance（m）	500-600
WiFi bridge distance (m)	2.4GHz: 600 5GHz: 400

Table 1. Lantern-Explorer detailed parameters

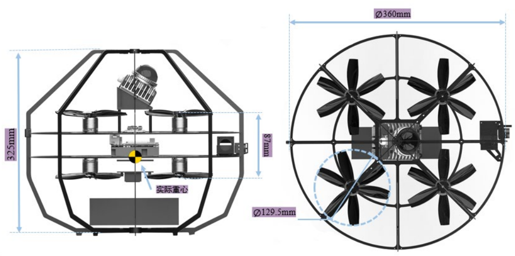

Figure 3. Lantern-Explorer 3D Dimension Diagram

3.2 Software Algorithm Optimization Design

3.2.1 Adaptive Odometry Accuracy Linear Controller

In the actual exploration process of the drone, as the frontier boundary points are updated, the planning algorithm frequently performs re-planning tasks, causing the direction and acceleration of the flight trajectory to change rapidly. This leads to divergence and localization drift in the laser-inertial odometry system (Lee et al., 2024). To ensure a balance between system efficiency and accuracy, we introduced an adaptive dynamic adjustment mechanism for the linear velocity within the controller between the flight control and planning algorithms. By real-time monitoring of the odometry's covariance matrix and the IMU's measurement errors, the controller output speed is dynamically adjusted. This allows the system to smoothly decelerate in situations with high localization uncertainty, ensuring the robustness and precision of the laser-inertial odometry. Specifically, the following dynamic constraints are applied to the linear velocities along the three coordinate axes, using the drone's body frame as a reference:

$$V_{adj} = V_{nor} \times \frac{1}{1+k_v \cdot trace(P_{position})} \tag{2}$$

V_{adj} is the linear velocity adjusted by the controller based on the covariance matrix, and V_{nor} is the nominal linear velocity. K_v is the adjustment coefficient used to control the sensitivity to current uncertainties. $trace(P_{position})$ is the trace of the position covariance matrix, representing the total uncertainty. Similarly, for angular velocity, we have:

$$\omega_{adj} = \omega_{nor} \times \frac{1}{1+k_v \cdot trace(P_{position})} \tag{3}$$

ω_{adj} is the angular velocity adjusted by the controller based on the covariance matrix, and ω_{nor} is the nominal angular velocity. K_v is the adjustment coefficient used to control the sensitivity to current uncertainties. $trace(P_{position})$ is the trace of the attitude covariance matrix.

Since real-time dynamic adjustments can lead to abrupt changes in velocity, which may potentially cause instability in the drone, we introduce a smoothing process based on a Low-Pass Filter (LPF) and second-order system response in the control strategy. For linear velocity V the adjusted velocity V_{adj} is input into a second-order filter to ensure smooth velocity changes. The transfer function of the second-order system is given by:

$$H(s) = \frac{h_n^2}{s^2+2\zeta h_n s+h_n^2} \tag{4}$$

h_n is the natural frequency, ζ is the damping ratio, and s is the complex frequency variable. The controller filters the velocity based on the following state-space equation:

$$\begin{aligned} \dot{x}_1 &= x_2 \\ \dot{x}_2 &= -2\zeta h_n x_2 - h_n^2 x_1 + h_n^2 v_{adj} \end{aligned} \tag{5}$$

x_1 represents the smoothed velocity V_{smooth}, and x_2 is an intermediate state variable that represents the rate of change of velocity. The output of this second-order system is the final smoothed velocity V_{smooth}.

Based on the combination of the above filter and controller, the system effectively smooths velocity changes during frequent re-planning processes, ensuring that the drone's flight trajectory remains stable and the stability of the laser-inertial odometry is further enhanced.

3.2.2 Improved FUEL-360

The FUEL algorithm, through the incremental frontier information structure (FIS) and hierarchical planning approach, enables rapid autonomous exploration of drones in complex environments(Zhou et al., 2010). The advantage of this algorithm lies in its integration of global path planning, local viewpoint optimization, and minimum time trajectory generation, allowing the drone to continuously and efficiently adapt to dynamic environments (as shown in figure 4(a)). To fully leverage the wide sensing range of LiDAR and improve both spatial exploration efficiency and mapping accuracy, this paper proposes the following main improvements to FUEL-360:

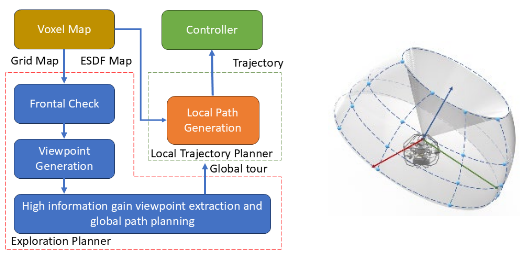

(a)FUEL360 Framework Diagram

(b) The Frontier Check of the LiDAR Field of View Model

Figure 4. Schematic of the FUEL-360 Algorithm Framework

3.2.3 Exploration Boundary Extraction and Viewpoint Generation with Integrated LiDAR FoV Model

FUEL uses the Intel Realsense D400 series stereo camera, which has a relatively short sensing range. In contrast, the LiDAR used by Lantern-Explorer has a range of 40 meters at 10% reflectivity. Directly applying the original algorithm limits the effective utilization of the LiDAR's wide sensing range, restricting its exploration efficiency in large-scale environments. Specifically, the point cloud from the LiDAR scan is first downsampled to reduce subsequent computational complexity. Then, based on the perception model, more reasonable viewpoints are generated, which can reduce redundant viewpoints, optimize the drone's exploration path, and avoid the repetitive viewpoint update process. By optimizing boundary extraction and viewpoint generation, exploration efficiency can be improved and redundant viewpoint selection reduced, as shown in figure 4(b). Define the horizontal field of view (FOV) of the LiDAR as θ_{LiDAR}, and the maximum detection range of the LiDAR as d_{max}. The frontier point set $P_{frontier}$ is defined as all points located at the boundary between the known and unknown regions. The optimization of the boundary point extraction is performed using the following formula:

$$P_{frontier} = \{p \in P_{scan} \mid \|p - p_{senor}\| = d_{max}, \theta_p \in [\theta_{min}, \theta_{max}]\} \tag{6}$$

Boundary points are calculated from the LiDAR scan data, and the extracted boundary points are clustered using Principal Component Analysis (PCA) to reduce redundant data. Additionally, the selection of viewpoints is based on the spatial distribution of the boundary points and the coverage area. The information gain $I(p)$ of a viewpoint p is defined as the coverage rate of the viewpoint, and the information gain formula is as follows:

$$I(p) = \sum_{q \in P_{frontier}} 1(line\ of\ sight\ from\ p\ to\ q) \tag{7}$$

3.2.4 Fusion of LiDAR FoV Model for Global Path Planning Optimization

To optimize the global path planning and reduce the frequent yaw angle adjustments caused by the narrow field of view (FOV) of stereo cameras, we introduce a weight function based on the LiDAR FOV to enhance the objective function. This helps minimize the impact of constant yaw adjustments, which can lead to accumulated errors and layer issues in the map during high-precision 3D mapping. The goal is to smooth the trajectory and improve the accuracy of the mapping process.

Specifically, we introduce a penalty term for yaw angle adjustments to optimize the global path planning objective. Let the drone move from its current position P_i to the next target position P_{i+1}, with yaw angles φ_i and φ_{i+1} at the respective positions. The path cost can be expressed as:

$$J_{path} = \sum_{i=1}^{N} \left(d(P_i, P_{i+1}) + \lambda_\varphi |\varphi_{i+1} - \varphi_i| \right) \tag{8}$$

$d(P_i,P_{(i+1)})$ represents the distance between consecutive viewpoints, and λ_φ is the weight coefficient for the change in yaw angle. By incorporating this formula, the objective is to minimize the yaw angle variation, thereby reducing the frequency of yaw adjustments.

3.2.5 Exploration Backtracking Optimization

In autonomous exploration, the FUEL algorithm typically prioritizes expanding the outermost regions, causing the drone to frequently return to previously explored areas to fill in unexplored parts, which increases path redundancy. To improve exploration efficiency, this paper references CMU's TARE planner (Cao et al., 2021), categorizing the boundaries into two types and prioritizing the first type to reduce backtracking. First, the boundaries are classified: Type 1 Boundary: Located inside the known area, forming a closed region. If a closed path can be found using the A* algorithm, it is defined as a Type 1 boundary. Exploring these boundaries usually requires only short-distance adjustments to quickly fill in gaps. Type 2 Boundary: Located outside the known area, typically open. Exploring these boundaries extends further and affects trajectory planning.
To reduce backtracking, this paper proposes two nested Traveling Salesman Problems (TSP):
Type 1 Boundary TSP: Prioritize exploring the unexplored regions inside the known area to fill in gaps.Type 2 Boundary TSP: After completing the internal exploration, extend to explore the external boundary.
Let P be the set of boundary points. The goal is to find the closed path with the minimum cost, prioritizing the unexplored areas inside the known region. Both types of P use the same objective function:

$$J_{TSP} = min \sum_{i=1}^{N} d(P_i, P_{i+1}) \tag{9}$$

4. Experiments and Analysis

Due to limitations in the actual testing environment, traditional drone flight trajectory evaluation methods based on motion capture are not feasible. Therefore, in this experiment, the relative spatial distances between six uniformly distributed laser retroreflective targets were used as ground truth data. The data were collected using a high-precision 3D laser scanner (model 5016) from the German company Z+F, which has a distance resolution of 0.1 mm, linear error less than 1 mm, and angular precision of 0.004° in both vertical and horizontal directions. The relative distances between the centers of the spheres, obtained by manually extracting the target regions and fitting spheres using the RANSAC algorithm, were used as the benchmark for map accuracy evaluation. The root mean square error (RMSE) was used as the primary metric for map accuracy assessment, calculated based on the relative distances between pairs of targets.

$$RMSE = \sqrt{\frac{2}{n(n-1)} \sum_{i=1}^{n-1} \sum_{j=i+1}^{n} \left(d_{ij} - d'_{ij} \right)^2} \tag{10}$$

4.1 Platform difference analysis

To separately assess the impact of the UAV platform's hardware and software optimization on the overall system's mapping accuracy, and to eliminate trajectory uncertainties introduced by autonomous and manual control flights, pre-defined waypoints were used for looped waypoint flights. The flight test trajectory is shown in figure 5.

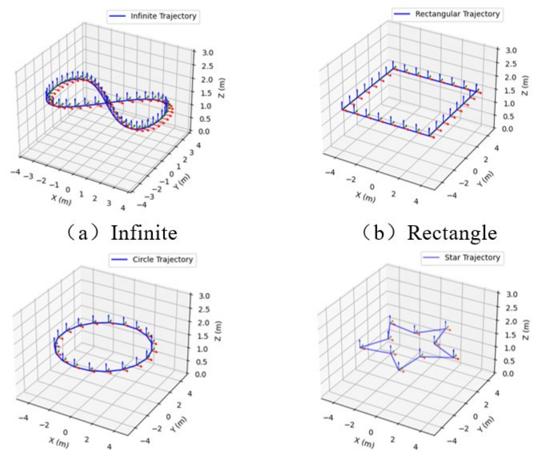

（a）Infinite （b）Rectangle
（c）Ring （d）Pentagram

Figure 5. Flight Test Trajectory Diagram

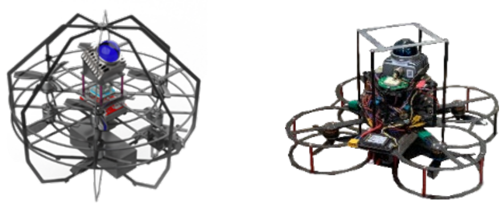

(a) Lantern-Explorer (b) QAV380

Figure 6. Comparison Test UAV Platform

For better comparison, the flight platform was equipped with a standard X4 structure collision-resistant drone, the QAV380 (shown in figure 6), as a benchmark. Both drones use the same motors and propellers and are equipped with the same Livox Mid-360 LiDAR. In all experiments, the controller output was limited to a maximum speed of 2.5 m/s and a maximum acceleration of 1 m/s². During the experiment, the drone sequentially traversed all waypoints. Each waypoint was predefined, and the control velocity and desired position, optimized dynamically by the Traj_server in Ego-Planner, were input into the controller. The relative distance error was calculated based on the Z+F scanner target ground truth. The final accuracy comparison was based on the average of five flight tests (Table 2).

UAV Platform	Controller adaptive constraints	RMSE (m) of relative distance error between targets			
		Infinite	Rectangular	Ring	Pentagram
Lantern-Explorer	Y	**0.031**	**0.047**	0.035	**0.071**
	N	0.092	0.079	0.049	0.137
QAV380	Y	0.046	0.051	**0.034**	0.081
	N	0.106	0.092	0.079	0.123

Table 2. Multi-Trajectory Flight Mapping Accuracy on Different Platforms

Table 2 shows that the Lantern-Explorer platform outperforms the QAV380 in mapping accuracy under controller-constrained conditions. The RMSE values for Lantern-Explorer are consistently lower than those of QAV380 across all flight paths, demonstrating better robustness and consistency in mapping accuracy. The RMSE for Lantern-Explorer ranges from 3.1 cm to 7.1 cm under controller constraints, while it increases significantly to 4.9 cm to 13.7 cm without them, highlighting the controller's significant impact on accuracy. The QAV380, especially without controller constraints, shows higher errors, with the RMSE reaching 10.6 cm on the Infinit path. Even with controller constraints, the QAV380's error remains higher than that of the Lantern-Explorer.

In terms of path influence, the RMSE for the Infinite trajectory is relatively low, especially when the controller adapts to constraints, with Lantern-Explorer showing only 3.1 cm error. The errors increase slightly on the Rectangular and Circle paths, particularly on the QAV380, where the RMSE reaches 9.2 cm and 7.9 cm, indicating that complex turns may make the platform's motion control more sensitive, affecting LiDAR data stability. The Star path shows the highest RMSE, likely due to sharp turns and nonlinear movements, which increase range errors. On Lantern-Explorer, the RMSE is 7.1 cm with constraints, rising to 13.7 cm without them. For QAV380, the controller's impact is also notable, but the RMSE remains high due to platform limitations; for instance, on the Circle path, the RMSE drops from 7.9 cm to 6.1 cm, still higher than Lantern-Explorer.

Overall, both platforms show improved accuracy with controller constraints, with the Lantern-Explorer's RMSE for the Rectangular path decreasing from 7.9 cm to 4.7 cm. This demonstrates the controller's effective control over platform dynamics, reducing motion errors and enhancing mapping accuracy. The results indicate that the Lantern-Explorer, with controller constraints, achieves superior mapping accuracy, especially in complex environments with multiple paths and sharp turns, where its error is notably lower than that of the QAV380.

4.2 Real-world scenario comparison experiment

To comprehensively validate the rationality and advancement of the hardware design and software optimization of the proposed system, several representative real-world scenarios were selected for comparison experiments, including tunnel, forest, underground corridor, and indoor environments. The evaluation metrics are the same as those in the previous section. In all experimental scenarios, the controller output was limited to a maximum speed of 1.5 m/s and a maximum acceleration of 0.5 m/s². Both drones used batteries of the same specifications, and the flight time was determined based on the time from takeoff until the battery reached low charge and the drone automatically landed or completed the exploration algorithm. The explored areas were processed in CloudCompare software to generate point cloud maps for further analysis. figure 7 is a schematic diagram of field environment testing.

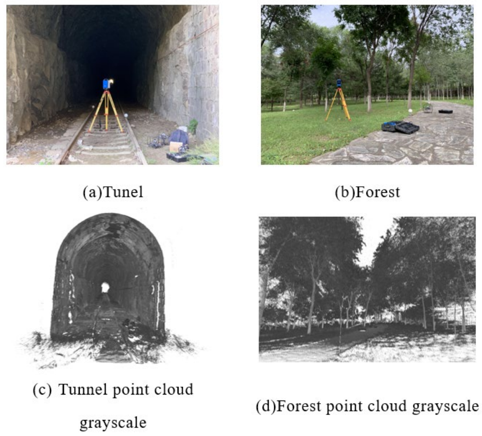

Figure 7. Data Collection Site Diagram

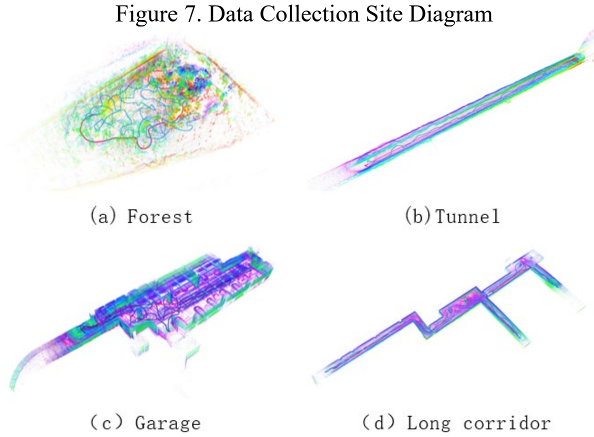

Figure 8. Actual Exploration Flight Trajectory Diagram

In this set of experiments, the Lantern-Explorer used the improved FUEL-360 and an adaptive accuracy linear controller, while the QAV380 employed the original FUEL and a basic PD controller for trajectory tracking based on the output of the planning algorithm. figure 8 shows the final point cloud maps built after exploration in the four environments. The red trajectory represents the exploration path of the Lantern-Explorer, while the blue trajectory represents the path of the QAV380.

We also recorded a comparison between the output speed of FUEL-360 (red curve) and the final output speed after the controller smoothing of the adaptive odometry accuracy in the forest scene (blue curve). As shown in figure 9, the speed variation from the planning algorithm's output is quite large, which is unfavorable for mapping. The blue curve represents the smoothed speed, which is the final output speed.

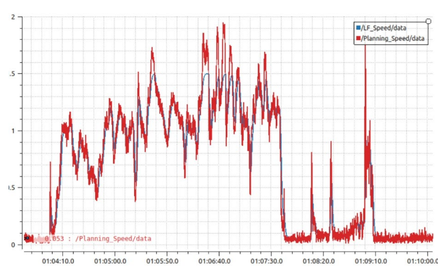

Figure 9. Comparison Curve of Planner Output Speed and Controller Output Speed

This contribution has been peer-reviewed. The double-blind peer-review was conducted on the basis of the full paper.
https://doi.org/10.5194/isprs-annals-X-G-2025-1077-2025 | © Author(s) 2025. CC BY 4.0 License.

UAV Platform	Scenario	Regional area（m^2）	Mapping accuracy (Target-to-target relative distance error RMSE (m))	Exploration area（m^2）	Exploration time (s)	Exploration efficiency (m^2/s)
Lantern-Explorer	Forest	~6700	0.118	~3000	512	5.86
	Tunnel	~1050	0.046	~950	252	3.77
	Garage	~800	0.037	~800	138	5.80
	Long corridor	~350	0.051	~350	240	1.46
QAV380	Forest	~6700	0.251	~2600	789	3.30
	Tunnel	~1050	0.092	~700	425	1.65
	Garage	~800	0.039	~800	126	6.35
	Long corridor	~350	0.060	~350	332	1.06

Table 3. Comparative Analysis of Autonomous Exploration Performance in Four Scenarios

Table 3 shows that the Lantern-Explorer platform outperforms the QAV380 in mapping accuracy (measured by RMSE of target relative distance) across all environments.

In the complex forest environment, the RMSE for Lantern-Explorer is 0.118 m, while for QAV380, it is 0.156 m. Due to dense tree coverage and frequent re-planning by the exploration algorithm, the exploration time and error increase. Lantern-Explorer maintains higher accuracy in such environments, indicating its system design is better suited for exploration and mapping in complex conditions.

In tunnel and underground parking scenarios, where the environment is more enclosed and structured, the planning algorithm path changes less. Lantern-Explorer keeps errors within 5 cm, with RMSE values of 0.046 m and 0.037 m, respectively, while QAV380 has slightly higher errors. These environments have lower external interference, allowing LiDAR to work stably, resulting in relatively low errors.

In the long corridor scenario, Lantern-Explorer's RMSE is 0.051 m, compared to 0.093 m for QAV380. The smooth corridor walls create a typical degraded scenario, resulting in larger errors in this environment.

In terms of exploration area and efficiency, Lantern-Explorer outperforms QAV380 across all scenarios. In the forest, Lantern-Explorer covered approximately 3000 m², while QAV380 only covered 2600 m². Lantern-Explorer's exploration speed is 5.86 m²/s, much higher than QAV380's 3.29 m²/s, showing that its laser LiDAR field-of-view model and viewpoint generation enable more efficient exploration in large environments.

In the tunnel and long corridor environments, Lantern-Explorer also performs better than QAV380. However, in the underground parking and long corridor environments, the efficiency difference is smaller due to the limited boundary extraction range in confined spaces. Despite the QAV380's adaptive odometry controller, Lantern-Explorer still demonstrates slightly higher overall performance.

5. Conclusions

This paper focuses on the hardware optimization design of collision-avoidance autonomous exploration drones, aiming to enhance their exploration and mapping capabilities in complex environments through a rational hardware architecture and software optimization. By integrating laser odometry technology, the paper provides an in-depth analysis and optimization design for various drone platforms, including hardware improvements in the power system layout, IMU data optimization, and control precision adjustments.

The hardware design introduces a drone platform architecture suited for complex environments, with a carefully designed power system and onboard sensor layout that effectively enhance stability and anti-interference capabilities. On the software side, an adaptive control algorithm based on dynamic constraints is introduced, along with an exploration algorithm that optimizes boundary extraction and viewpoint generation by integrating LiDAR characteristics. Additionally, boundary classification reduces the problem of exploration retracing, significantly improving the drone's localization and mapping accuracy in dynamic environments.

Experiments in four representative scenarios—forest, tunnel, underground parking garage, and long corridor—demonstrate that the optimized drone platform outperforms traditional solutions in both exploration efficiency and mapping accuracy, particularly in complex environments like forests and underground garages. The Lantern-Explorer platform shows significant improvements in mapping accuracy and consistently higher exploration efficiency than the QAV380 platform across different scenarios. Furthermore, by comparing RMSE errors across different flight paths, the study verifies the effective improvement in mapping accuracy, with the controller's adaptive function significantly reducing errors caused by motion during exploration.

In conclusion, the proposed hardware and software optimization design successfully enables efficient exploration and precise mapping of drones in complex environments, providing valuable design insights for future collision-avoidance autonomous exploration drone systems. Future work could focus on hardware lightweighting, algorithm complexity optimization, and integrating visual semantic information to further enhance drone performance in practical applications.

Acknowledgements

This work was supported by the National Key R&D Program of China (Grant No. 2022YFB3904101), the National Natural Science Foundation of China (Grant No. 42071444), and the Beijing Imaging Theory and Technology High-End Innovation Center Special Fund.

References

Baca, T., Petrlik, M., Vrba, M., et al., 2021. The MRS UAV System: Pushing the Frontiers of Reproducible Research, Real-world Deployment, and Education with Autonomous Unmanned

Aerial Vehicles. *Journal of Intelligent & Robotic Systems*, 102(1), 26-54. doi:10.1007/s10846-021-01383-5.

Bohorquez, F., 2007. Rotor hover performance and system design of an efficient coaxial rotary wing micro air vehicle. [Ph. D. thesis]. University of Maryland, College Park, Maryland, United States.

Bondyra, A., Gardecki, S., Gąsior, P., Giernacki, W., 2016. Performance of coaxial propulsion in design of multi-rotor UAVs. Challenges in Automation, Robotics and Measurement Techniques. ICA 2016. Advances in Intelligent Systems and Computing, 440, 523-531. Springer International Publishing. doi.org/10.1007/978-3-319-29357-8_46.

Bristeau, P. J., Martin, P., Salaün, E., Petit, N., 2009. The role of propeller aerodynamics in the model of a quadrotor UAV. In 2009 European control conference (ECC) , 683-688. IEEE. doi: 10.23919/ecc.2009.7074482.

Cao, C., Zhu, H., Choset, H., Zhang, J., 2021. TARE: A Hierarchical Framework for Efficiently Exploring Complex 3D Environments. In Robotics: Science and Systems, 5(2). doi: 10.15607/rss.2021.xvii.018.

Chen, J.Y., Shi, Y.C., 2019. Research progress in solid-state LiDAR. *Opto-Electronic Engineering*, 46(7), 47-57. doi: 10.12086/oee.2019.190218.

Foehn, P., Kaufmann, E., Romero, A., Penicka, R., Sun, S., Bauersfeld, L., Laengle, T., Cioffi, G., Song, Y., Loquercio, A., & Scaramuzza, D., 2022. Agilicious: Open-source and open-hardware agile quadrotor for vision based flight. *Science robotics*, 7(67), eabl6259. doi.org/10.1126/scirobotics.abl6259.

Gomez, C., Hernandez, A.C., Barber, R., 2019. Topological Frontier-Based Exploration and Map-Building Using Semantic Information. *Sensors*, 19(20), 4595-4615. DOI:10.3390/s19204595

Gul, F., Mir, I., Gul, U., et al., 2023. A Review of Space Exploration and Trajectory Optimization Techniques for Autonomous Systems: Comprehensive Analysis and Future Directions. International Conference on Pervasive Knowledge and Collective Intelligence on Web and Social Media. Cham: Springer Nature Switzerland. doi:10.1007/978-3-031-31469-8_9.

Kim, B., Azhari, M.B., Park, J., Shim, D.H., 2024. An autonomous UAV system based on adaptive LiDAR inertial odometry for practical exploration in complex environments. *Journal of Field Robotics*, 41(3), 669-698. doi.org/10.1002/rob.22284.

Kong, F., Xu, W., Cai, Y., et al., 2021. Avoiding Dynamic Small Obstacles With Onboard Sensing and Computation on Aerial Robots. IEEE Robotics and Automation Letters, 6(4), 7869-7876. doi:10.1109/lra.2021.3101877.

Lee, D., Jung, M., Yang, W., et al., 2024. LiDAR odometry survey: recent advancements and remaining challenges. Intelligent Service Robotics, 17(2), 95-118. doi:10.1007/s11370-024-00515-8.

Peng, X., Su, G., Sengupta, R., 2024. An autonomous Unmanned Aerial Vehicle exploration platform with a hierarchical control method for post-disaster infrastructures. *IET Cyber-Systems and Robotics*, 6(1). doi.org/10.1049/csy2.12107.

Wallace, L., Lucieer, A., Watson, C., et al., 2012. Development of a UAV-LiDAR System with Application to Forest Inventory. *Remote Sensing*, 4(6), 1519-1543. doi:10.3390/rs4061519.

Wang, B., Liu, K., Jia, Y., Lu, L., 2024. Research on unmanned aerial vehicle inspection system for transmission lines based on laser radar. In 2024 3rd International Conference on Energy, Power and Electrical Technology (ICEPET), 890-893. IEEE. doi.org/10.1109/icepet61938.2024.10626020.

Wang, C., Morris, J.T., Smith, E.M., 2024. A Lidar Biomass Index of Tidal Marshes from Drone Lidar Point Cloud. *Remote Sensing*, 16(11), 1823-1837. doi.org/10.3390/rs16111823.

Yamauchi, B., 1997. A frontier-based approach for autonomous exploration. In Proceedings of the 1997 IEEE International Symposium on Computational Intelligence in Robotics and Automation CIRA'97 , 146-151. doi:10.1109/cira.1997.613851.

Zhang, Y., Chen, X., Liu, P., Wang, J., Zou, H., Pan, N., Shen, S., 2024. UniQuad: A Unified and Versatile Quadrotor Platform Series for UAV Research and Application. IEEE Conference on Robotics and Automation (ICRA-X40). doi.org/10.48550/arXiv.2407.00578.

Zhou, B., Zhang, Y., Chen, X., et al., 2020. FUEL: Fast UAV Exploration using Incremental Frontier Structure and Hierarchical Planning. IEEE Robotics and Automation Letters, 6(2), 779-786. doi.org/10.1109/LRA.2021.3051563.

Zhou, X., Wang, Z., Ye, H., Xu, C., Gao, F., 2020. Ego-planner: An esdf-free gradient-based local planner for quadrotors. IEEE Robotics and Automation Letters, 6(2), 478-485. doi.org/10.1109/LRA.2020.3047728.

Zhu, H., Cao, C., Xia, Y., et al., 2021. DSVP: Dual-Stage Viewpoint Planner for Rapid Exploration by Dynamic Expansion. In Proceedings of the 2021 IEEE/RSJ International Conference on Intelligent Robots and Systems (IROS), 7623-7630. doi:10.1109/iros51168.2021.9636473.